



**HAL**  
open science

## Global optimization of metasurface designs using statistical learning methods

Mahmoud M R Elsayy, Stéphane Lanteri, Régis Duvigneau, Gauthier Brière, Mohamed Sabry Mohamed, Patrice Genevet

► **To cite this version:**

Mahmoud M R Elsayy, Stéphane Lanteri, Régis Duvigneau, Gauthier Brière, Mohamed Sabry Mohamed, et al.. Global optimization of metasurface designs using statistical learning methods. 2019. hal-02156881v1

**HAL Id: hal-02156881**

**<https://hal.science/hal-02156881v1>**

Preprint submitted on 14 Jun 2019 (v1), last revised 1 Dec 2019 (v3)

**HAL** is a multi-disciplinary open access archive for the deposit and dissemination of scientific research documents, whether they are published or not. The documents may come from teaching and research institutions in France or abroad, or from public or private research centers.

L'archive ouverte pluridisciplinaire **HAL**, est destinée au dépôt et à la diffusion de documents scientifiques de niveau recherche, publiés ou non, émanant des établissements d'enseignement et de recherche français ou étrangers, des laboratoires publics ou privés.

# Statistical learning approaches for the design of highly efficient gradient metasurfaces at visible regime

Mahmoud M. R. Elsawy,<sup>1,\*</sup> Stéphane Lanteri,<sup>1</sup> Régis Duvinneau,<sup>1</sup> Peiman Ni,<sup>2</sup> Gauthier Brière,<sup>2</sup> and Patrice Genevet<sup>2</sup>

<sup>1</sup>*Université Côte d'Azur, Inria, CNRS, LJAD, 06902 Sophia Antipolis Cedex, France*

<sup>2</sup>*CNRS, CRHEA, Université Côte d'Azur, rue Bernard Gregory, Sophia Antipolis, Valbonne, France*

(Dated: June 14, 2019)

In this work, we exploit two advanced optimization techniques based on statistical learning and evolutionary strategies together with a fullwave high order Discontinuous Galerkin Time-Domain (DGTD) solver in order to optimize 3D gradient metasurfaces with different shapes. Unlike what is usually provided in the literature, first we introduce rigorously to the community the methodologies of our advanced optimization techniques that outperform most of the available techniques in the literature, especially for complex problems that contain several global minima/maxima. Second, we demonstrate both numerically and experimentally optimal designs for 3D real life gradient metasurfaces based on GaN semiconductor at the visible regime. Our numerical results reveal that for spherical shaped antenna, one can achieve more than 85% of diffraction efficiency for both TM and TE polarization using only 150 solver runs. In addition, for rectangular shaped antenna, an efficiency above 88% can be achieved for TM polarization using less than 150 fullwave simulations. To the best of our knowledge, this is the highest diffraction efficiency reported so far at the visible regime for real life 3D structures.

**PACS numbers:** 78.67.Pt, 02.30.Zz, 02.60.Pn, 82.20.Wt

## INTRODUCTION

Metasurfaces have been studied extensively in the past few years due to their exceptional abilities in achieving full light control in a very short propagation distance at any desired direction thanks to the simplified fabrication procedures compared to bulk metamaterials [1–6]. Metasurfaces consist of an array of subwavelength nanoresonator arrays with spatially varying geometric parameters and subwavelength separation, made of plasmonic [4, 7] and/or high dielectric refractive index materials [6, 8]. Unlike the conventional optical components that provide a full control of the light properties over a long propagation distances, metasurfaces can achieve a full control of the phase, amplitude, and wavefront in a very short propagation distance much smaller than the wavelength and with very high resolution [3–9].

Owing to the versatility and the capabilities of metasurfaces, many exotic and peculiar optical phenomena ranging from negative refraction [10], sub-diffraction optical microscopy [11], and broadband achromatic lenses [12] have been demonstrated recently using ultrathin and compact devices. Most of these designs have been engineered using a direct modelling approach, that is metasurface parameters are tuned using costly parametric studies. However, due to the complexity of the real life problems that include large parameter space in the metasurface design, the direct modelling approach becomes insufficient [13, 14] and the use of an inverse design technique is mandatory to achieve the maximum desired performance [14, 15]. Several optimization methodologies have been developed and demonstrated for the de-

sign of metasurfaces in the recent years, including local and global search methods. The former, converges faster, however, they can be stuck in local maxima/minima due to the strong dependence on the initial guess [16]. This category includes topology optimization [17–20] and so-called *objective-first* algorithms [21–23].

The global optimization techniques including stochastic search techniques like genetic algorithms [24–26] and evolutionary algorithms [27, 28] are more general and are suitable for optimizing large parameter space. However, most of these techniques require large number of forward solver calls, which make them inapplicable for modelling 3D designs, that require costly simulations and include large parameter search space.

In the last two years, artificial neural networks have been used to develop innovative modelling strategies for several nanoscale light-matter interaction problems including solving the light scattering from a spherical nanoshell [29] and have also been leveraged to design efficient metasurface devices [30, 31]. As a general rule, in order to train a network, one has to generate numerous training data. Once the network is trained, it can be used to achieve the optimized design based on a specific input target. However, in order to build an efficient neural network, one needs to generate thousands of training data using a fullwave electromagnetic solver, that require of course significant computational time [32, 33] especially for 3D complex problems. Another common problem for the neural networks is the diversity of the parameters which might lead to poor performance of the network. In other words, one might obtain for the same input data, different structures that meet the same response. In this case, the performance of the network is reduced dramatically [31, 32].

The main goal of our work is twofold. First, we

---

\* mahmoud.elsawy@inria.fr

introduce to the metasurface community two different advanced optimization techniques based on statistical learning approaches that outperform most of optimization techniques used in the inverse design of metasurfaces (especially when considering 3D problem setups). We adopt a shape optimization viewpoint as opposed to a topology optimization approach for instance. Our methods converge fastly to a global minima/maxima even if the modelling parameter space is relatively large (with regards to a shape optimization setting). In addition, as we will show here, our methods are able to obtain effectively different global minima/maxima that have the same value of the objective function, but with different parameter values (an analytical example is provided to give the reader more insights). The second goal of this paper is to apply these techniques in order to optimize 3D gradient metasurface with different shapes based on GaN semiconductor in order to achieve a maximum light deflection efficiency at wavelength  $\lambda = 600 \text{ nm}$ . We choose GaN semiconductor due to its negligible losses and due to its high refractive index in the visible regime, which yields ideal nanoresonators (phase-shifters) for metasurface designs [8, 34]. In fact, several metasurface designs have been demonstrated both numerically and experimentally for light deflection at near infrared [20, 27, 35] using silicon or hydrogenated amorphous silicon. Nevertheless, due to the absorption losses of silicon at visible regime, a  $\text{TiO}_2$  [18] or c-Si [18, 36] based metagratings have been used to demonstrate efficient light deflection at visible regime. However, the efficiency does not exceed 80% [37].

Here, we provide optimal 3D metasurface designs with efficiency above 87%. To the best of our knowledge, this is the highest efficiency reported in the literature at visible regime for 3D gradient metasurface designs. Using our efficient global optimization techniques which based respectively on advanced evolution strategies and statistical learning, together with our rigorous Discontinuous Galerkin Time Domain (DGTD) solver from the DIOGENES software suite dedicated to computational nanophotonics [38] we propose optimal gradient metasurface designs with rectangular and spherical shaped antennas that provide maximum diffraction efficiency ( $\eta(n, m)$ , where  $n, m$  are the mode indices) at  $\lambda = 600 \text{ nm}$ . For rectangular shaped antenna, we show that one can achieve more than 87% of diffraction efficiency at  $\lambda = 600 \text{ nm}$  for TM polarized waves. Second, for spherical shaped antenna, we show that one can achieve more than 85% for both TM and TE light polarization at  $\lambda = 600 \text{ nm}$ .

## RESULTS AND DISCUSSION

We use two different efficient global optimization techniques based respectively on advanced evolution strategies and statistical learning. The first one is the covariance matrix adaptation evolution strategy (CMA-

ES) [39]. The CMA-ES has been gaining a lot of attention since it requires fewer cost function evaluations compared to the other evolutionary algorithms like genetic algorithms (GA) [15, 24] especially for 3D designs that require expensive simulations. The second method is the Efficient Global Optimization (EGO) algorithm [40]. The EGO algorithm is based on the surrogate modelling [40] in order to reduce dramatically the computational cost (number of calls for the electromagnetic solver).

In order to understand how the CMA-ES works, let us first revisit the meaning of an optimization evolutionary strategy. The evolutionary strategy can be seen as an algorithm that provides the user a set of candidate parameter values (solution to the problem), these solutions will be used to compute the values of the objective function. Based on these values of the current solutions, the algorithm will then produce the next generation of candidate solutions (using some learning approaches), that is more likely to produce even better values for the objective functions than the current generation. The size of the population range from problem to another. However, most of the classical evolutionary strategies consider a fixed population size at each iteration. In another words, the search parameters are chosen first and remain without changing during the optimization process. This main drawback of the classical evolutionary strategies make the choice of the parameter depends strongly on the considered problem and might lead to expensive and costly computations at each iteration. The most common evolutionary strategy in the electromagnetic community is the Genetic Algorithm (GA) [41]. This technique has been used to optimize the performance of several electromagnetic problems [24, 25, 41, 42]. However, this method require a substantial amount of time even if with the high-performance capabilities of the electromagnetic solvers [42]. Therefore, due to the huge number of parameters required to ensure the flexibility of the modern devices, it is preferable to find a better evolutionary strategies that offer faster convergence (require less calls for the solver) and provide accurate results.

The CMA-ES has been gaining a lot of attention recently, since it requires fewer cost function evaluations compared to the classical evolutionary algorithms like GA. The CMA-ES operates by reshaping and moving a Gaussian distribution in all the search space in order to find the global minimum [13, 39, 43]. This Gaussian distribution is fully defined by its mean and its shape is defined by the covariance matrix. The CMA-ES is able to adapt itself and adjust the search parameters during the optimization by changing the shape and the size of the search distribution at each iteration according to the progress (see Fig. 1(a) for a simple illustration). This advanced evolutionary strategy uses several internal parameters to adapt itself and generally it behaves like a black-box optimizer. One needs just to choose the initial population size, a random initial guess and the algorithm attempts to make best progress in a few number of iteration by changing the shape and the size of the search

space at each iteration in order to find the global minima/maxima as illustrated in Fig. 1(a). Consequently, the CMA-ES requires fewer solver calls compared to the classical evolutionary strategies like GA [15, 24] in which the shape of the distribution and the size of the search space remain constant during optimization process that might lead to costly simulation compared to CMA-ES. For more details about CMA-ES, the reader can refer to Refs. [13, 39, 43].

Despite, the advantageous of the CMA-ES over all the evolutionary optimization strategies, for large parameter space problems, the CMA-ES still require costly simulations. To overcome this issue, the use of surrogate models in the framework of statistical learning is a promising approach. In particular, in our work we focus on the Efficient Global Optimization (EGO) algorithm. The EGO algorithm is a global optimization algorithm based on the surrogate modelling, that is to say, replacing the complex or costly evaluation process by a simpler and cheaper model [40, 44] to reduce dramatically the computational cost (number of calls for the electromagnetic solver). The EGO uses a statistical learning process in order to drive the optimization [40, 44] and it is based on two phases. The first one is the Design Of Experiment (DOE), in which an initial database (with the bounded search space for the parameters) is generated. In another words, for random parameter values (corresponds to different metasurface designs), the cost function is evaluated using an electromagnetic solver. In the second phase, using the data obtained from the DOE, a Gaussian process model is constructed to fit these data. This Gaussian model, allows us to predict the values of the cost function in the search parameter space. Using a specific merit function (expected improvements in our case), the most interesting points (parameter values) that correspond to a maximum expected improvements are selected. These new points are then simulated using the solver to compute the new objective function and the error estimations, then another Gaussian model, will be constructed using the new objective function evaluations. We repeat this process until we reach a predefined convergence criterion, or when the expected improvement is very small. A flow chart of the EGO procedure can be found in Fig. 1(b). In order to show the different behaviors of CMA-ES and EGO, we provide a 2D analytical example to illustrate the principle ideas of both methods. We consider the minimization of a 2D Branin function

$$\begin{cases} \underset{x,y}{\text{minimize}} f(x,y) = \left( y - \frac{5.1}{4\pi^2}x^2 + \frac{5}{\pi}x - 6 \right)^2 \\ \quad + 10 \left( 1 - \frac{1}{8\pi} \right) \cos(x) + 10, \\ \text{subject to } -5 \leq x \leq 10 \text{ and } 0 \leq y \leq 15. \end{cases} \quad (1)$$

The Branin function  $f(x,y)$  has 3 global minima, i.e three different combination of  $x$  and  $y$  generate the same value of the objective function, as it is indicated by the black arrows in Fig. 1(c). The main idea here, we want

show the different behaviors of CMA-ES and EGO. We start by the CMA-ES, as we mentioned above, the CMA-ES starts with an initial point (initial parameter values), and adapt itself during the optimization by changing the shape and the size of the search distribution. The yellow points shown in Fig. 1(d) represent the values of the objective function evaluation during the CMA-ES optimization, as it can be seen, the CMA-ES converges to one global minima in an efficient way, however it took nearly 180 iterations to get one global point as it is shown in Fig. 1(e) where the convergence is clearly illustrated. On the other hand, the EGO method represented by the black points in Fig. 1(d), is able to catch all the three global points, and then tries to enrich the data around one of them to get a better value. For the EGO, we consider an initial DOE including 5 points (blue points in Fig. 1(f)), then a Gaussian model is constructed using this DOE, and after only 35 iterations (including DOE), the EGO was able to visit all the three global minima as illustrated by the black points in Fig. 1(d) and Fig. 1(f). This analytical example shows the powerful of each method and also illustrates the different mechanism of each of them in optimizing the problems. In the following we will use the CMA-ES and EGO in order to optimize different metasurface geometries in order to maximize the deflection light efficiency at  $\lambda = 600 \text{ nm}$ .

As a first example, in Fig. 2(a), we consider a gradient based metasurface made of rectangular GaN semiconductor (dark-red regions) placed over a semi-infinite substrate made of  $\text{Al}_2\text{O}_3$  (shown in green). We consider a normal incident plane-wave with electric field polarized in the  $y$ -direction, and we aim to maximize the diffraction efficiency of the first order mode  $\eta(0, -1)$  (deflect light in the same plane of incidence  $y$ - $z$  plane) at wavelnegth  $\lambda = 600 \text{ nm}$ . Thus, we consider a sub-wavelength period in the  $x$ -direction ( $300 \text{ nm}$ ) to limit the diffraction into the substrate, and we consider a period of  $1500 \text{ nm}$  in the  $y$ -direction, as it can be seen in Fig. 2(a). In this first design, we consider a rectangular shaped antennas, in which the positions of each ridges in  $y$  direction and thicknesses in  $x$  and  $y$  directions, together with the height of the ridges need to be optimized. The 12 optimized parameters are represented by the red circles in Fig. 2(a). It is worth mentioning that we took into account the experimental constraints during the optimization process, in which the minimum feature size is set to  $90 \text{ nm}$  and the height of the ridges is set between  $600 \text{ nm}$  and  $800 \text{ nm}$ .

In Fig. 2(b-c), we present the results obtained using our optimization techniques for optimizing the rectangular shaped metasurface shown in Fig. 2(a). The CMA-ES results are shown in Fig. 2(b), in which the objective function evaluation at each iteration is shown in dark-yellow points, the best values of the objective function at each iteration is represented by the purple solid curve. In principal, at each generation, we evaluate 11 metasurface designs and the best value is kept if it is better than the best one obtained in the previous generation. As we can see, after nearly 550 iterations, we obtain

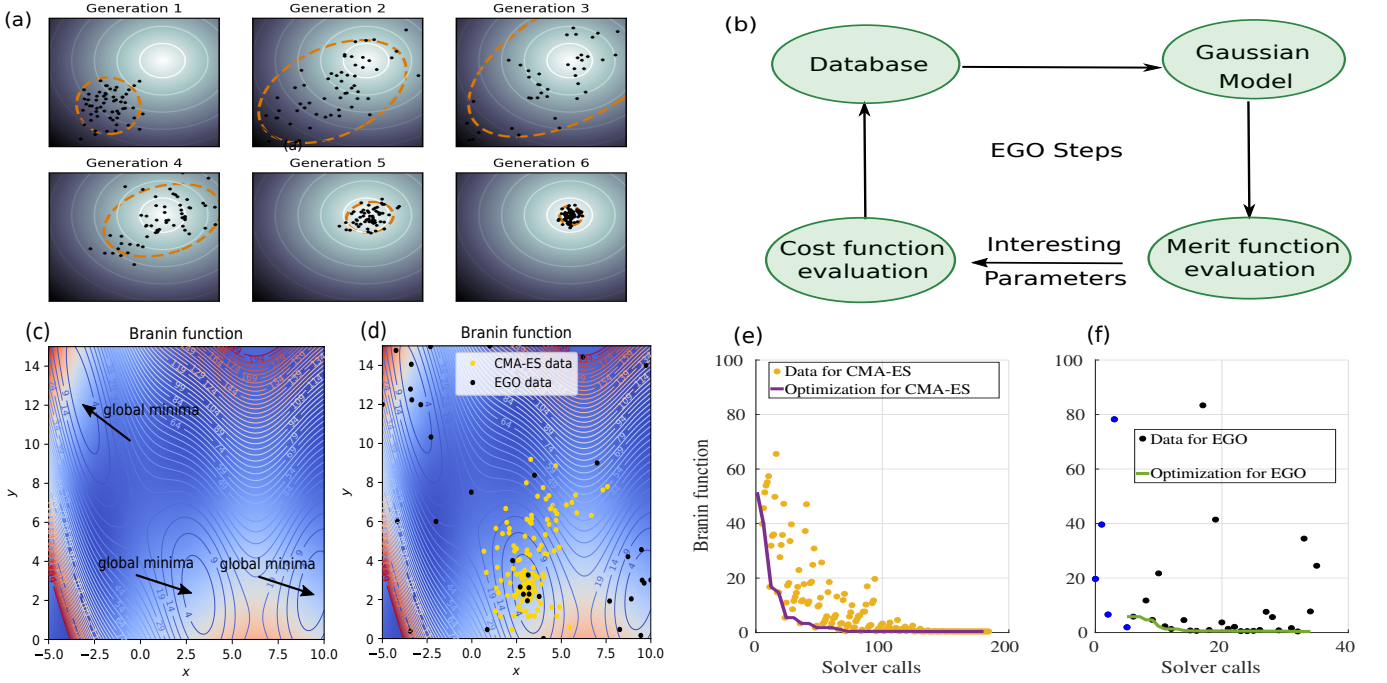


FIG. 1. (a): simple illustration of the CMA-ES method (this figure is captured from wikipedia). (b): schematic diagram for the EGO steps. (c-d): 2D example to illustrate the different behaviors of CMA-ES and EGO methods. We consider here the minimization of a the Branin function that has 3 global minima indicated by the black arrows in (c). The CMA-ES and the EGO results are given in (d). The evolution of CMA-ES as a function of the solver calls is provided in e, the yellow points represent the objective function values at each iterations, the purple curve indicates the best value at each iteration. (f): similar to (e) except that here the blue points represent the DOE and the black ones give the data during the optimization. See the text for more explanation.

a global minima such that  $1 - \eta^{TM}(0, -1) \approx 0.119$  at  $\lambda = 600 \text{ nm}$ , which is corresponding to diffraction efficiency of approximately 88.10% for TM polarized waves. The evolution of the diffraction efficiency  $\eta^{TM}(0, -1)$  as a function of the wavelength is represented by the purple curve in Fig. 2(d), in which the maximum is achieved at  $\lambda = 600 \text{ nm}$ . The corresponding parameter values is shown in the left purple table in Fig. 2(e), where  $dx$  and  $dy$  give the thickness in  $x$  and  $y$  directions, respectively for each rectangular element, and  $h$  denotes the height of the ridges (see Fig. 2(a)). As it can be seen from this table, that we have a usual gradient thicknesses in  $y$  direction that will provide gradual light deflection in  $y$ - $z$  plane. In addition, the height of the ridges is nearly  $800 \text{ nm}$ , which is long enough to provide longitudinal modes to propagate in  $z$  direction and achieve an efficient light delay. The field maps for the  $Re(H_x)$  and  $Re(E_y)$  at  $\lambda = 600 \text{ nm}$  can be found in Fig. 2(f) and Fig. 2(g), respectively, where the light deflection is clearly demonstrated. It is worth mentioning that during the optimization process, we consider a coarse mesh consisting of 3000 cells with fourth order polynomial  $P_4$  (thanks to our DGTD solver [38]) which is sufficient to obtain accurate results. The convergence proof is provided in Fig. 5(a) in the supplementary information section. Here, the results shown in Figs. 2(d) and Figs. 2(f-g) are obtained using

thin mesh with second order polynomial  $P_2$  for better field visualization.

Now, we move to the results obtained by the EGO method for optimizing the rectangular metasurface shown in Fig. 2(a). As we have stated before, the first phase of the EGO model is to obtain a DOE. In this example, we consider 80 random points to construct the DOE represented by the blue points in Fig. 2(c). Based on these 80 points, a surrogate model is constructed and is used during the optimization process to find a global minimum below the best point found in the DOE process (represented by the pink point in Fig. 2(c)). As it can be seen from the green curve and its associated data (black points just above the green curve Fig. 2(c)), the convergence is obtained after a few number of iterations (after that the curve is flat meaning that according to the investigated data the best point has been obtained). We stop the simulation after only 150 iterations (solver calls including the DOE) since this minimization level of the cost function is sufficient for us and we converge to a global minimum in which  $1 - \eta(0, -1) \approx 0.12$  which corresponds to a deflection efficiency of 88.0% at  $\lambda = 600 \text{ nm}$ . In other words, using the EGO, we optimized 12 parameters and obtained a diffraction efficiency around 88.0% at  $\lambda = 600 \text{ nm}$  using only 150 solver calls which is much smaller than the number of solver calls

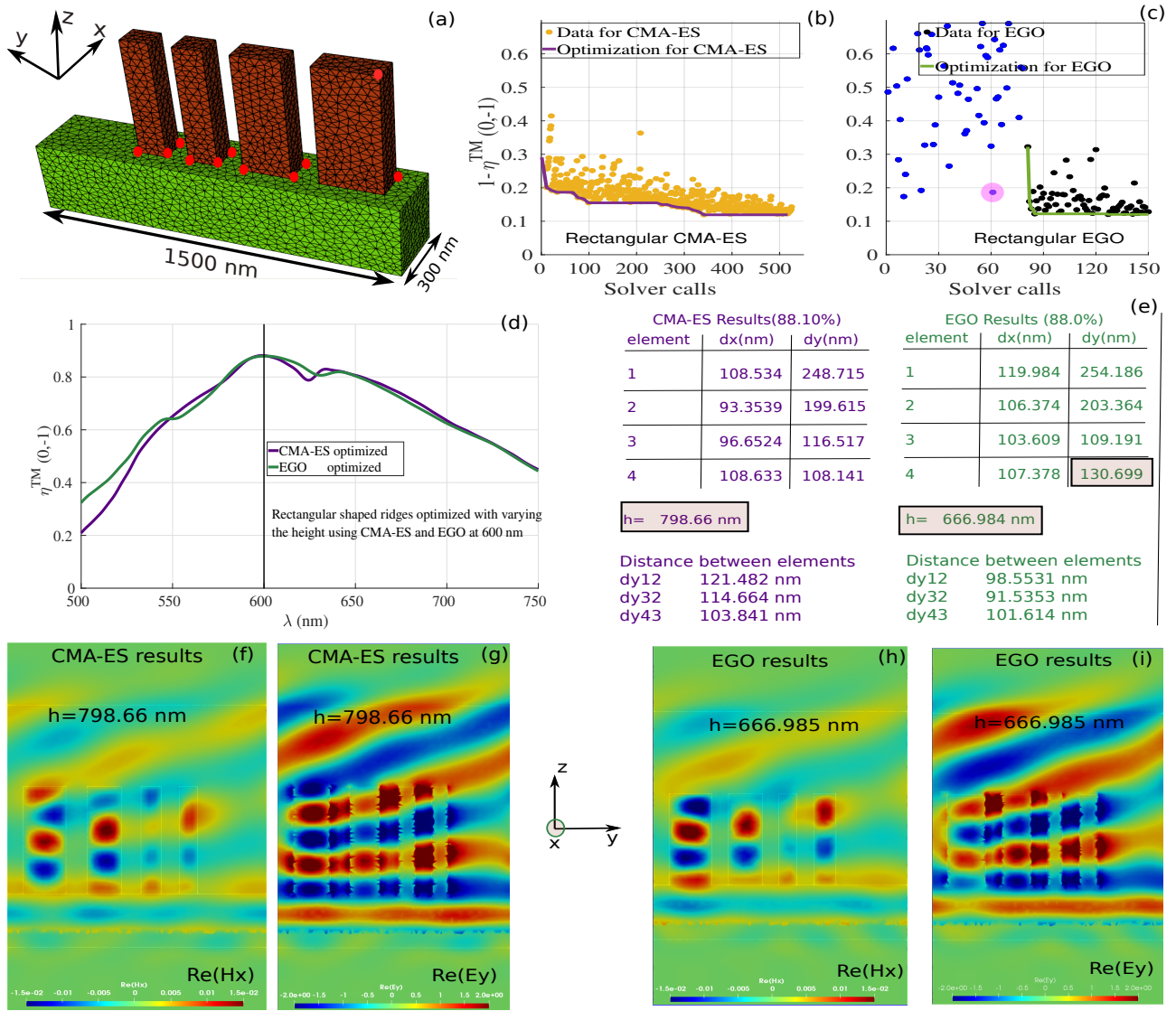


FIG. 2. Results for rectangular shaped antenna. (a): the geometry under consideration with rectangular nano ridges made of GaN (dark-red ridges) on top of a semi-infinite substrate made of  $\text{Al}_2\text{O}_3$  (green region). The 12 red circles represent the optimization parameters. (b): optimization process using CMA-ES as a function of the solver calls. Dark-yellow points represent the value of the objective function at each iteration, the solid purple line gives the best point during the optimization up to the current iteration. (c): optimization using the EGO as a function of the solver calls. The blue points represent the DOE, the black points represent the value of the objective function at each optimization iteration, and the green solid line indicates the optimized data. (d): comparison between the diffraction efficiency for the first order mode as a function of the wavelength for the TM polarized wave. Purple and green colors for the CMA-ES and EGO optimized geometries, respectively; the corresponding parameter values shown in (e). (f-i): field maps for  $\Re(H_x)$  and  $\Re(E_y)$  for the optimized geometries at  $\lambda = 600\text{ nm}$ .

used in the CMA-ES procedure (see Fig. 2(b)). Interestingly, the optimized parameters obtained by the EGO method (up to our stopping criteria) are different from the one found by the CMA-ES method (see Fig. 2(e)), even if both of them provide nearly the same diffraction efficiency 88% at  $\lambda = 600\text{ nm}$  as in is inferred in Fig. 2(d). Obviously, for the results obtained by the EGO method (right green table in Fig. 2(e)), the gradient in the  $d_y$  thicknesses of the ridges is not fully satisfied ( $d_y$  for the last ridge is bigger than the one before), unlike the re-

sults obtained by the CMA-ES. In addition, the height of the nanoridges is much shorter than the one found by the CMA-ES method (nearly one wavelength). This means that up to 150 solver calls, the EGO has obtained another global point that is not found by the CMA-ES, similar to what we have seen before for the analytical example shown in Fig. 1(c-d). In addition, this is also can be understood from the field maps provided in Figs. 2(h-i), in which we clearly see that the number of longitudinal modes propagates for the optimized geometry found

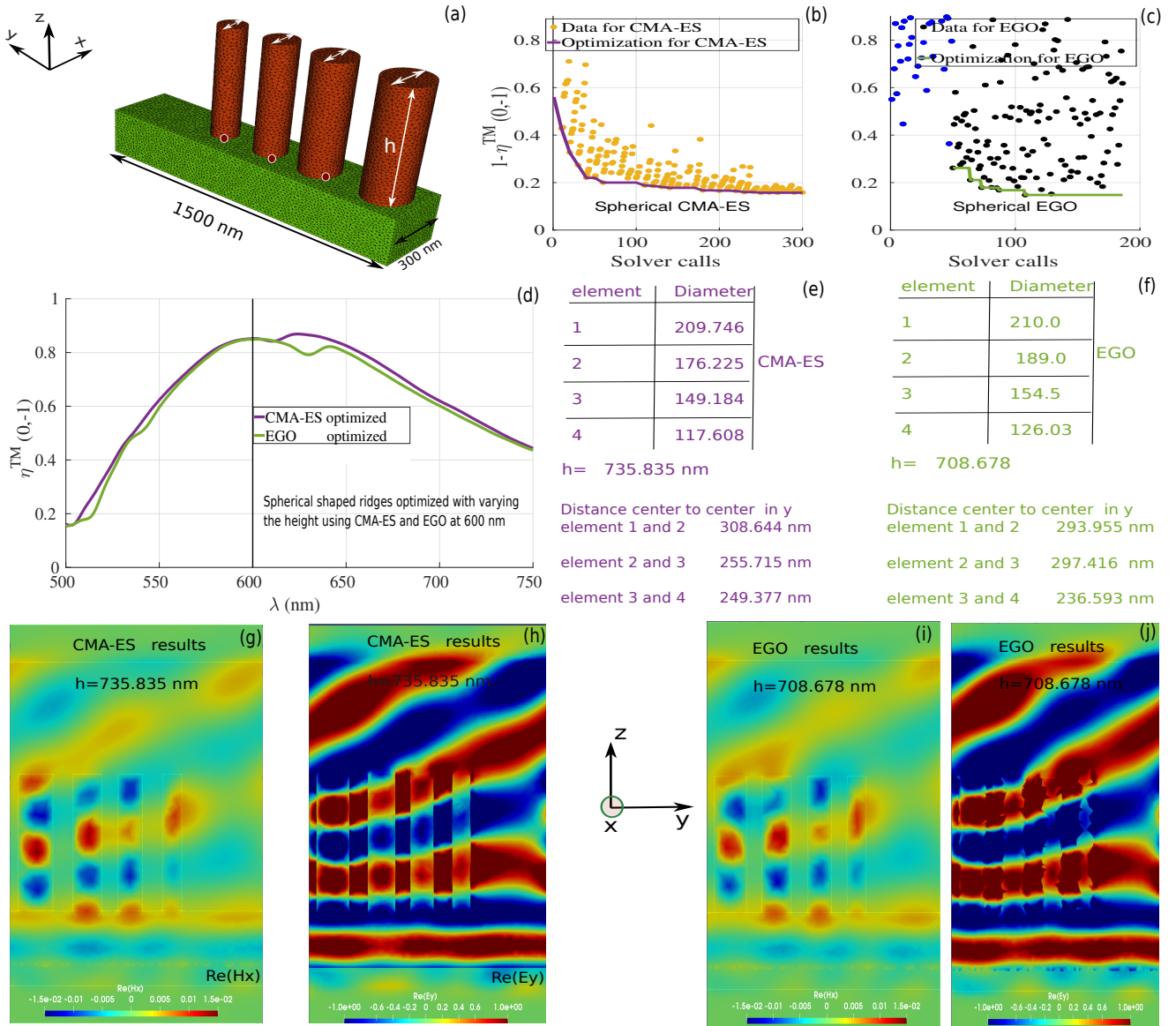


FIG. 3. Results for spherical shaped antenna. Similar to Fig.2, (a): the geometry under consideration with spherical nano ridges made of GaN (dark-red ridges) on top of a semi-infinite substrate made of  $\text{Al}_2\text{O}_3$  (green region). The 8 red circles represent the optimization parameters. (b): optimization process using CMA-ES as a function of the solver calls. Dark-yellow points represent the value of the objective function at each iteration, the solid purple line indicates the best point during the optimization up to the current iteration. (c): optimization using the EGO as a function of the solver calls. The blue points represent the DOE, the black points represent the value of the objective function at each optimization iteration, and the green solid line indicates the optimized data. (d): comparison between the diffraction efficiency for the first order mode as a function of the wavelength for the TM polarized wave. Purple and green colors for the CMA-ES and EGO optimized geometries, respectively; the corresponding parameter values shown in (e-f). (g-j): field maps for  $\Re(H_x)$  and  $\Re(E_y)$  for the optimized geometries at  $\lambda = 600$  nm.

by the EGO are different from the ones obtained by the CMA-ES (see Figs. 2(f-g)), which explains why we have at least two different global minima in this configuration, which is an evident proof that the CMA-ES and EGO are two different efficient and complementary optimization techniques. We would like to emphasize here that in our design, we consider a unit cell made of 4 nanoridges, rather than optimizing a single ridge (as it is always the

case for most of the works available in the literature), since the coupling between the modes propagating in the nanoridges cannot be negligible (see Figs. 2(g) and 2(i)). This coupling is of great importance, and must be taken into account during the optimization process in order to provide a robust design with small fabrication error as we shall see in our future work. This coupling could be another reason to explain why we obtained different global

minima in our design.

As a second example, we use our optimization methods to optimize a metasurface made of spherical nano antennas (see Fig. 3(a)) in order to maximize the diffraction efficiency for the first order mode as for the rectangular case shown above, but insensitive to the polarization change unlike the rectangular shape. In this case, we optimize 8 parameters (see Fig. 3(a)) we optimize the diameter of each ridges (thick white arrows), the height, and the position of the ridges represented by the red points. We consider the same experimental constraints as for the rectangular case.

We begin again with the CMA-ES results shown in Fig. 3(b), similar to the rectangular case, we obtain a global point after 300 solver calls with diffraction efficiency around 85% for TM polarized waves (results for TE polarization is also around 85%, data not shown). For the EGO, we consider a DOE of 50 points (see blue points in Fig. 3(b)), after that a Gaussian model is constructed and a global point is clearly obtained with nearly 180 iterations with efficiency 85%. Nevertheless, even if we have gradient in the diameter thicknesses for the two set of geometries, the two set of parameters obtained by CMA-ES and EGO are slightly different (see Figs. 3(e-f)). In addition, the evolution of the efficiency as a function of the wavelength is again slightly different. This can be understood again from the field maps obtained at  $\lambda = 600 \text{ nm}$ , in which they are similar except for the number of longitudinal mode is slightly different. Here for the CMA-ES results we obtain  $h = 735.835 \text{ nm}$ , and we see nearly half of the last mode loop in the first ridge, however, for the results obtained from the EGO, we see a very small part of the last mode loop in the first ridge. This can be understood from the small different in height between the two set of parameters which is about  $30 \text{ nm}$ . In order to give more insight about this results, in Fig. 4, we consider optimizing the geometry shown in Fig. 3(a), but with fixed height  $h = 800 \text{ nm}$ , using the CMA-ES and compare the results with the ones obtained with the CMA-ES with varying the height. In Fig. 4(a), one clearly sees that the results obtained with fixed height  $h = 800 \text{ nm}$  approaches the results obtained with varying the height. Moreover, the set of parameters obtained from both of them are quite similar to each other. This also can be seen from field maps in Figs. 4(e-f), in which for the geometry with  $h = 800 \text{ nm}$ , the last mode loop in the first ridge is completely inside the ridge, which provides more phase delay and slightly higher efficiency at  $\lambda = 600 \text{ nm}$  as it is shown in Fig. 4(d). The convergence proof of the spherical case can be found in the supplementary information in Fig. 5(b), in which we investigated different mesh sizes and different polynomial orders. It is worth mentioning that during the optimization process, we used a coarse mesh of 10000 cells with fourth order polynomial  $P_4$  which is sufficient to get accurate results especially at  $\lambda = 600 \text{ nm}$  (the desired wavelength) as it is depicted in Fig. 5(b). However, all the results obtained for the optimized geometry shown in Figs. 3(g-i) and 4(g-

j) are obtained with thin mesh of 109000 cells and second order polynomial order  $P_2$  for better field visualization. In Fig. 5(b) Thanks to our DGTD solver, we are able to use show even more accurate results using higher order curveliniar elements with different higher order polynomial, in order to provide more accurate numerical results for the comparison with our future experimental work.

Based on our numerical results shown above for both the rectangular and spherical shaped antennas, it is clear that the CMA-ES and EGO, "understood" that there is a key parameter that has the biggest influence on the minimization process. Here, we clearly see that for all the results obtained above the optimizers try to set the thickness of the first ridge ( $d_y$  in case of rectangular and diameter in case of spherical shaped antennas) to the maximum. Which also make sense from the physical point of view, so as to achieve a gradient phase delay in  $y$ - $z$  plane and maximize the deflection efficiency for the first order mode. The second parameter which is important, is the height of the ridges, due to the different numbers of longitudinal modes that can lead to the same diffraction efficiency (taking into account the full coupling between the ridges). The other parameters has also impact on the deflection efficiency, but less than the thickness of the first parameter and also the height of the ridges. This is again a clear evidence that our optimization methods provide meaningful results that can be interpreted from the physical point of view. From the fabrication point of view, the structures with  $h = 800 \text{ nm}$ , are more favorable for us and they will be considered in our future work for the fabrication and the characterization processes.

## CONCLUSION

Two advanced optimization techniques based on statistical learning approach (EGO) and on advanced evolutionary strategies (CMA-ES) have been introduced and used in order to optimize 3D metasurface. These methods are widely used in the computational fluid dynamics community, but here we introduce them to the metasurface community, and prove that they are very efficient in obtaining different global minima/maxima using acceptable electromagnetic solver calls. We applied these methods in order to maximize the light deflection efficiency at  $\lambda = 600 \text{ nm}$  using GaN based metasurfaces. Our numerical results reveal that one can obtain 85% of deflection efficiency for both TM and TE polarization using cylindrical shaped antennas. In addition, we show that using rectangular shaped antennas, one might obtain more than 88% of deflection efficiency for TM polarization. Based on the field maps obtained from our rigorous DGTD solver, we provide physical insights about the optimized geometries. The fabrication and the characterization of the optimized geometries will be presented in our future work.

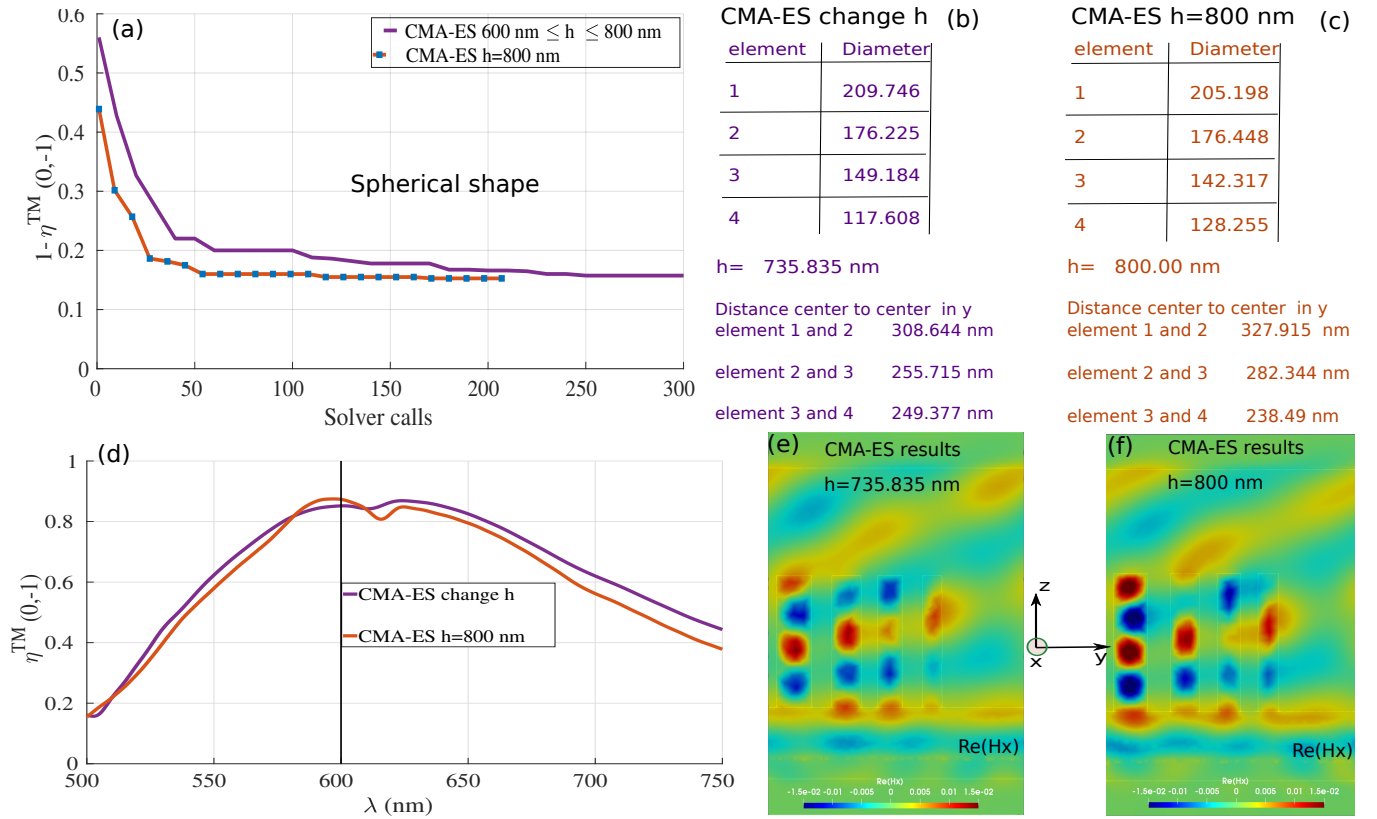


FIG. 4. (a): comparison between results obtained with CMA-ES (for the spherical shaped antenna) with changing height (purple curve, see Fig. 3 (b)), and the ones obtained with CMA-ES with fixed  $h = 800 \text{ nm}$  as a function of the solver calls. The corresponding optimized parameter values shown in (b-c). (d): diffraction efficiency as a function of the wavelength. (e-f): field maps for  $\Re(H_x)$  at  $\lambda = 600 \text{ nm}$ .

## ACKNOWLEDGEMENTS

This research was funded by the European Research Council (ERC) under the European Union's Horizon 2020 research and innovation programme (Grant agreement no. 639109).

## AUTHOR CONTRIBUTIONS

M.M.R.E conducted the simulation. R.D developed the optimization methods. P.G and S.L proposed the structure. M.M.R.E, R.D, and S.L analysed the optimization results. M.M.R.E, P.N, G.B, and P.G analysed the physical results. M.M.R.E, R.D, S.L, and P.G wrote the manuscript. All authors reviewed the manuscript.

## APPENDIX

In Fig.5, we present the numerical convergence for some of the optimized geometries shown above. In

Fig.5(a), we study the influence of the mesh and the polynomial order on the optimized solution obtained in the rectangular case (the results obtained from the CMA-ES shown in Fig.2). As it can be seen in Fig.5(a), using fourth order polynomial order with a coarse mesh (only 3000 cells) provides the same results when we consider second order polynomial order with thin mesh (with 147000 cells). Fig.5(b), we show the convergence for the cylindrical case using both linear elements and also curvilinear higher order elements. As it can be noticed, the convergence achieved with less cells in the case of the curvilinear elements compared to the case with linear ones (due to the feature of the cylindrical shaped antennas). To conclude on this point, thanks to our DGTD solver, we are able to prove the convergence for the optimized geometries using different mesh size and/or types, which is not trivial especially for the case of cylindrical elements that require higher order curvilinear mesh type for more accurate results.

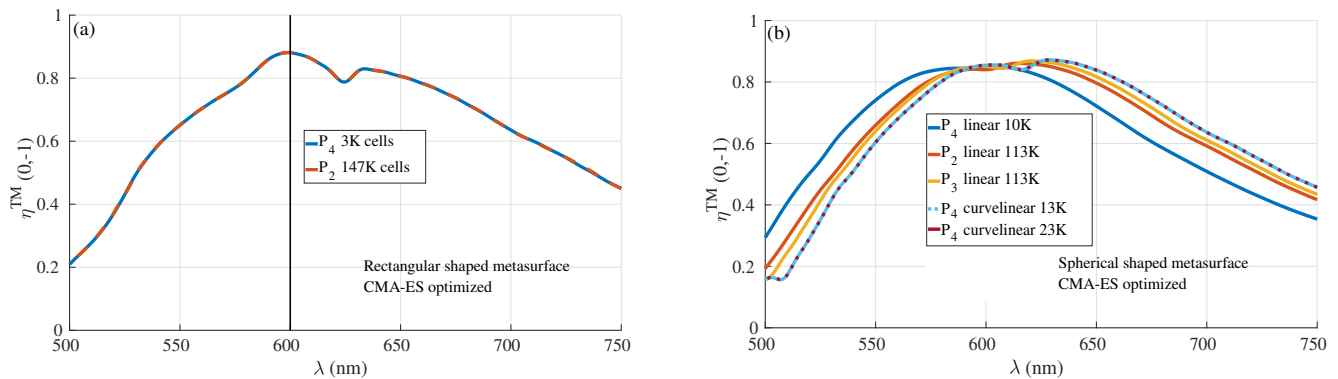


FIG. 5. Convergence study (a): for the rectangular shaped antenna with coarse mesh and fourth order polynomial  $P_4$  (blue curve) and with thin mesh with second order polynomial  $P_2$  (purple curve). (b): convergence results for the spherical shaped antenna, with coarse mesh and  $P_4$  (blue curve), with different mesh sizes, different polynomial orders, and different mesh types.

- [1] Simion Astilean, Philippe Lalanne, Pierre Chavel, Edmond Cambril, and Huguette Launois. High-efficiency subwavelength diffractive element patterned in a high-refractive-index material for 633?? nm. *Optics letters*, 23(7):552–554, 1998.
- [2] Philippe Lalanne, Simion Astilean, Pierre Chavel, Edmond Cambril, and Huguette Launois. Design and fabrication of blazed binary diffractive elements with sampling periods smaller than the structural cutoff. *JOSA A*, 16(5):1143–1156, 1999.
- [3] Nanfang Yu, Patrice Genevet, Mikhail A. Kats, Francesco Aieta, Jean-Philippe Tetienne, Federico Capasso, and Zeno Gaburro. Light propagation with phase discontinuities: Generalized laws of reflection and refraction. *Science*, 334(6054):333–337, 2011.
- [4] Xingjie Ni, Naresh K. Emani, Alexander V. Kildishev, Alexandra Boltasseva, and Vladimir M. Shalaev. Broadband light bending with plasmonic nanoantennas. *Science*, 335(6067):427–427, 2012.
- [5] Shulin Sun, Qiong He, Shiyi Xiao, Qin Xu, Xin Li, and Lei Zhou. Gradient-index meta-surfaces as a bridge linking propagating waves and surface waves. *Nature materials*, 11(5):426, 2012.
- [6] Dianmin Lin, Pengyu Fan, Erez Hasman, and Mark L. Brongersma. Dielectric gradient metasurface optical elements. *Science*, 345(6194):298–302, 2014.
- [7] Alexander Y Zhu, Arseniy I Kuznetsov, Boris Luk'yanchuk, Nader Engheta, and Patrice Genevet. Traditional and emerging materials for optical metasurfaces. *Nanophotonics*, 6(2):452–471, 2017.
- [8] Patrice Genevet, Federico Capasso, Francesco Aieta, Mohammadreza Khorasaninejad, and Robert Devlin. Recent advances in planar optics: from plasmonic to dielectric metasurfaces. *Optica*, 4(1):139–152, Jan 2017.
- [9] Mane-Si Laure Lee, Ph Lalanne, JC Rodier, P Chavel, E Cambril, and Y Chen. Imaging with blazed-binary diffractive elements. *Journal of Optics A: Pure and Applied Optics*, 4(5):S119, 2002.
- [10] D. R. Smith, Willie J. Padilla, D. C. Vier, S. C. Nemat-Nasser, and S. Schultz. Composite medium with simultaneously negative permeability and permittivity. *Phys. Rev. Lett.*, 84:4184–4187, May 2000.
- [11] Alessandro Salandrino and Nader Engheta. Far-field sub-diffraction optical microscopy using metamaterial crystals: Theory and simulations. *Phys. Rev. B*, 74:075103, Aug 2006.
- [12] Shuming Wang, Pin Chieh Wu, Vin-Cent Su, Yi-Chieh Lai, Mu-Ku Chen, Hsin Yu Kuo, Bo Han Chen, Yu Han Chen, Tzu-Ting Huang, Jung-Hsi Wang, et al. A broadband achromatic metalens in the visible. *Nature nanotechnology*, 13(3):227, 2018.
- [13] Kenneth Diest, editor. *Numerical Methods for Metamaterial Design*, volume 127 of *Topics in Applied Physics*. Springer Netherlands, Dordrecht, 2013.
- [14] Kan Yao, Rohit Unni, and Yuebing Zheng. Intelligent nanophotonics: merging photonics and artificial intelligence at the nanoscale. *Nanophotonics*, 2018.
- [15] Sean Molesky, Zin Lin, Alexander Y Piggott, Weiliang Jin, Jelena Vuckovic, and Alejandro W Rodriguez. Outlook for inverse design in nanophotonics. *arXiv preprint arXiv:1801.06715*, 2018.
- [16] Jianji Yang and Jonathan A. Fan. Topology-optimized metasurfaces: impact of initial geometric layout. *Optics Letters*, 42(16):3161, August 2017.
- [17] Jakob Søndergaard Jensen and Ole Sigmund. Topology optimization for nano-photonics. *Laser & Photonics Reviews*, 5(2):308–321, 2011.
- [18] David Sell, Jianji Yang, Sage Doshay, Kai Zhang, and Jonathan A Fan. Visible light metasurfaces based on single-crystal silicon. *ACS Photonics*, 3(10):1919–1925, 2016.
- [19] David Sell, Jianji Yang, Sage Doshay, and Jonathan A Fan. Periodic dielectric metasurfaces with high-efficiency, multiwavelength functionalities. *Advanced Optical Materials*, 5(23):1700645, 2017.
- [20] David Sell, Jianji Yang, Evan W Wang, Thaibao Phan, Sage Doshay, and Jonathan A Fan. Ultra-high-efficiency anomalous refraction with dielectric metasurfaces. *ACS Photonics*, 5(6):2402–2407, 2018.
- [21] Alexander Y. Piggott, Jesse Lu, Thomas M. Babinec, Konstantinos G. Lagoudakis, Jan Petykiewicz, and Jelena Vučković. Inverse design and implementation of a

- wavelength demultiplexing grating coupler. *Scientific Reports*, 4(1), May 2015.
- [22] F. Calletwaert, V. Velez, P. Kumar, A. V. Sahakian, and K. Aydin. Inverse-Designed Broadband All-Dielectric Electromagnetic Metadevices. *Scientific Reports*, 8(1), December 2018.
- [23] Logan Su, Rahul Trivedi, Neil V. Saprà, Alexander Y. Piggott, Dries Verduyck, and Jelena Vučković. Fully-automated optimization of grating couplers. *Optics Express*, 26(4):4023, February 2018.
- [24] Victor Egorov, Michal Eitan, and Jacob Scheuer. Genetically optimized all-dielectric metasurfaces. *Optics Express*, 25(3):2583–2593, 2017.
- [25] Samad Jafar-Zanjani, Sandeep Inampudi, and Hossein Mosallaei. Adaptive genetic algorithm for optical metasurfaces design. *Scientific reports*, 8(1):11040, 2018.
- [26] Alexej V Pogrebniyakov, Jeremy A Bossard, Jeremiah P Turpin, J David Musgraves, Hee Jung Shin, Clara Rivero-Baleine, Nikolas Podraza, Kathleen A Richardson, Douglas H Werner, and Theresa S Mayer. Reconfigurable near-ir metasurface based on ge 2 sb 2 te 5 phase-change material. *Optical Materials Express*, 8(8):2264–2275, 2018.
- [27] Krupali D. Donda and Ravi S. Hegde. Rapid design of wide-area heterogeneous electromagnetic metasurfaces beyond the unit-cell approximation. *Progress In Electromagnetics Research M*, 60:1–10, 2017.
- [28] Peter R Wiecha, Arnaud Arbouet, Christian Girard, Aurélie Lecestre, Guilhem Larrieu, and Vincent Paillard. Evolutionary multi-objective optimization of colour pixels based on dielectric nanoantennas. *Nature nanotechnology*, 12(2):163, 2017.
- [29] John Peurifoy, Yichen Shen, Li Jing, Yi Yang, Fidel Cano-Renteria, Brendan G DeLacy, John D Joannopoulos, Max Tegmark, and Marin Soljačić. Nanophotonic particle simulation and inverse design using artificial neural networks. *Science advances*, 4(6):eaar4206, 2018.
- [30] Sandeep Inampudi and Hossein Mosallaei. Neural network based design of metagratings. *Applied Physics Letters*, 112(24):241102, 2018.
- [31] Zhaocheng Liu, Dayu Zhu, Sean Rodrigues, Kyu-Tae Lee, and Wenshan Cai. A generative model for the inverse design of metasurfaces. *Nano letters*, 2018.
- [32] Dianjing Liu, Yixuan Tan, Erfan Khoram, and Zongfu Yu. Training deep neural networks for the inverse design of nanophotonic structures. *ACS Photonics*, 5(4):1365–1369, 2018.
- [33] Mohammad H Tahersima, Keisuke Kojima, Toshiaki Koike-Akino, Devsh Jha, Bingnan Wang, Chungwei Lin, and Kieran Parsons. Deep neural network inverse design of integrated nanophotonic devices. *arXiv preprint arXiv:1809.03555*, 2018.
- [34] Nikolai Schmitt, Niklas Georg, Gauthier Brière, Dimitrios Loukrezis, Sébastien Héron, Stéphane Lanteri, Charalambos Klitis, Marc Sorel, Ulrich Römer, Herbert De Gerssem, Stéphane Vézian, and Patrice Genevet. Optimization and uncertainty quantification of gradient index metasurfaces. *Opt. Mater. Express*, 9(2):892–910, Feb 2019.
- [35] David Sell, Jianji Yang, Sage Doshay, Rui Yang, and Jonathan A Fan. Large-angle, multifunctional metagratings based on freeform multimode geometries. *Nano letters*, 17(6):3752–3757, 2017.
- [36] Zhenpeng Zhou, Juntao Li, Rongbin Su, Beimeng Yao, Hanlin Fang, Kezheng Li, Lidan Zhou, Jin Liu, Daan Stellinga, Christopher P Reardon, et al. Efficient silicon metasurfaces for visible light. *ACS Photonics*, 4(3):544–551, 2017.
- [37] Philippe Lalanne, Simion Astilean, Pierre Chavel, Edmond Cambri, and Huguette Launois. Blazed binary subwavelength gratings with efficiencies larger than those of conventional échelette gratings. *Optics letters*, 23(14):1081–1083, 1998.
- [38] *Diogenes: A Discontinuous-Galerkin based software suite for nano-optics*. <https://diogenes.inria.fr/>.
- [39] N. Hansen, S.D. Muller, and P. Koumoutsakos. Reducing the time complexity of the derandomized evolution strategy with covariance matrix adaptation (cma-es). *Evolutionary Computation*, 11(1):1–18, 2003.
- [40] D.R. Jones. A taxonomy of global optimization methods based on response surfaces. *Journal of Global Optimization*, 21:345–383, 2001.
- [41] Randy L Haupt and Douglas H Werner. *Genetic algorithms in electromagnetics*. John Wiley & Sons, 2007.
- [42] R.L. Haupt. An introduction to genetic algorithms for electromagnetics. *IEEE Antennas and Propagation Magazine*, 37(2):7–15, April 1995.
- [43] N. Hansen and A. Ostermeier. Completely derandomized self-adaptation in evolution strategies. *Evolutionary Computation*, 9(2), 2001.
- [44] D.R. Jones. Efficient global optimization of expensive black-box functions. *Journal of Global Optimization*, 13(4), 1998.